

**“Large Scale Physical Modelling Study of a Flexible Barrier under
the Impact of Granular Flows” (nhess-2018-131)**

Reply to Review Comments from the Editor

by Dao-yuan TAN and Co-Authors

The authors wish to thank the handling editor for his insightful and constructive comments on the manuscript and advice to us for improving the quality of the paper. The authors have taken full consideration of all those comments and made clarification and corrections in following tables:

No.	Editor’s comments	Reply
1	Thank you for your response, please address the comments of the reviewers in an updated version.	Reply: Thank you for your reminder, all the comments of the reviewers and corresponding revisions have been addressed in the updated version in the attached files using black underlined fonts.
2	Very important that you address the issues of the Cd (drag coefficient) as I think most practicing engineers are interested in this value. Please note that a recent paper has been published in this field in the Canadian Geotechnical Journal: https://doi.org/10.1139/cgj-2016-0157 .	Reply: This suggestion is very valuable and helpful to improve the draft: nhess-2018-131. The published paper by Wendeler <i>et al.</i> (2018) reviewed previous laboratory tests (Wendeler and Volkwein 2015) and full-scale field tests (Berger <i>et al.</i> 2011; Wendeler 2008) and proposed a stepwise load model to estimate the impact forces on the flexible barrier during the interaction with a debris flow. The hydro-dynamic approach and the hydro-static approach were applied in that model. The hydro-dynamic approach with the dynamic coefficient $c_w=2.0$ for granular flows suggested in that literature can accurately evaluate the impact forces on the flexible ring net measured in our large-scale tests. This literature also assumed that the impact loading from a debris flow applied on a flexible barrier is evenly distributed over the barrier. This assumption was proved by back-calculation using the data of field tests, which supports the assumption made in our draft that the impact pressure in the measured area can reflect the impact loading on the impact area of the flexible ring net (see Page 14 Lines 327-330). To improve the quality of the draft: nhess-2018-131, the suggested literature has been comprehensively reviewed and appropriately cited. The revised and added contents are

		<p>marked as blue underlined fonts in the revised draft:</p> <ol style="list-style-type: none"> 1) Page 3-4 (Lines 77-82). 2) Page 4-5 (Lines 102-104). 3) Review of the literature in Page 6 (Lines 132-144). 4) Page 6 (Lines 147-148). 5) Page 11 (Lines 267-272). 6) The compared hydro-dynamic approaches with the test results used the dynamic coefficients proposed by Wendeler (2008): $c_w=2.0$ for granular flows and $c_w=0.7$ for debris flows with lower densities to verify their application in predicting impact forces of dry granular flows. See Page 17 (Lines 405-407), Page 18 (Lines 412-423) and Table 3 (Page 27). 7) Add the suggested paper into the reference list: Page 24 (Lines 576-578).
--	--	---

References:

- Berger, C., McArdell, B.W., Schlunegger, F. (2011). Direct measurement of channel erosion by debrisflows, Illgraben, Switzerland. *J. Geophys. Res.* 116, F01002, doi: 10.1029/2010JF001722: 18 p.
- Wendeler, C. S. I. (2008). Murgangrückhalt in Wildbächen. Grundlagen zu Planung und Berechnung von flexiblen Barrieren. ETH.
- Wendeler, C., Volkwein, A., McArdell, B.W. and Bartelt, P. (2018). Load model for designing flexible steel barriers for debris flow mitigation. *Canadian Geotechnical Journal*, (ja).
- Wendeler, C., and Volkwein, A. (2015). Laboratory tests for the optimization of mesh size for flexible debris-flow barriers. *Natural Hazards and Earth System Sciences*, 15(12).

**“Large Scale Physical Modelling Study of a Flexible Barrier under
the Impact of Granular Flows” (nhess-2018-131)**

Reply to Review Comments from the Referees

by Dao-yuan TAN and Co-Authors

The authors wish to thank the referees for their insightful and constructive comments on the manuscript and advice to us for improving the quality of the paper. The authors have taken full consideration of all those comments and made clarification and corrections in following tables:

No.	Referee 1's comments	Reply
1	How did the authors define the word large-scale in their experiments?	Reply: This is a very good question. The definition of large-scale in our tests (PolyU model) is based on the definition of the large-scale physical model built by USGS (Iverson <i>et al.</i> 2010; Iverson 2015). The physical model built in PolyU site has similar dimensional parameters to the USGS debris-flow flume. Specifically, the capacity of testing material is 5 m ³ in PolyU model compared to 10 m ³ in USGS flume, and the width of the flume is 1.5 m in PolyU model compared to 2 m in USGS flume. Even though the length of the flume in PolyU model is much shorter than the length of USGS flume (7 m compared to 95 m), the flume in PolyU model is sufficient to generate debris flows with dynamic parameters similar to real cases. In the trial tests, the generated watery flood can reach a velocity higher than 8 m/s during the flowing down. In the generated granular flow, the flow velocity (5 m/s), the measured impact force (10.96 kN) and the deposition mechanism are similar to the parameters of debris flows in literatures (Bugnion and Wendeler 2010; Arattano and Marchi 2005). Thus, we regard Polyu model as a large-scale physical model. Related explanation has been added into the manuscript in Page 8 (Lines 179-189).

2	<p>In lines 195-197, how did the authors define the deposition height of the granular flow, and the maximum horizontal deformation of the flexible barrier? It is better to show them in the scratch.</p>	<p>Reply: Thanks for the valuable comment, we have added the definitions of the deposition height and the maximum horizontal deformation of the flexible barrier in Page 10, Lines 239-242 and Fig.5 in Page 33.</p>
3	<p>What are the unique advantages of the experiments performed in this paper compared to the other researches, as the authors stated that an improved large-scale physical modelling facility for debris flow research has been conducted?</p>	<p>Reply: The description of the improved large-scale physical model is to emphasize that the physical modelling device is improved by a fast door opening system (see Page 7, Line 168). With the fast door opening system, the door can be flipped up quickly (shorter than 0.5 s) after triggering to minimize the interference from the door and increase the uniformity of the generated granular flows. Besides, a new method is utilized to directly measure the impact forces on the flexible ring net (Section 4.1), which is another advantage of the experiment device in this paper.</p>
4	<p>How many Test1 and Test2 experiments were performed by the authors? It would be great if the authors can comment how the experimental results vary between different rounds of experiments.</p>	<p>Reply: Thanks for the comments, and we only did once for each test. We will consider conducting more tests in the future by changing parameters of granular flows and flexible barriers. However, it is difficult to perform more tests within a short period due to the long preparation time of each test.</p>
5	<p>In Table 1, how did the authors determine the internal friction angle and the interface friction angle for granular flows?</p>	<p>Reply: The internal friction angle of the aggregates, which is regarded having the same value with the angle of repose (Hutter and Koch 1991), is measured by the pouring test introduced by Miura <i>et al.</i> (1997) and Zhou <i>et al.</i> (2014). The interface friction angle is determined by the tilting plane method introduced by Hutter and Koch (1991) and Zhou <i>et al.</i> (2014). The above description has been added in the manuscript (Page 9, Lines 217-221).</p>
6	<p>In the 4th column of Table 3, the unit kN should not be italic.</p>	<p>Reply: Noted with thanks, we have corrected it in the manuscript.</p>

References

- Arattano, M. and Marchi, L., (2005). Measurements of debris flow velocity through cross-correlation of instrumentation data. *Natural Hazards and Earth System Science*, 5(1), 137-142.
- Bugnion, L. and Wendeler, C., (2010). Shallow landslide full-scale experiments in combination with testing of a flexible barrier. *WIT Transactions on Engineering Sciences*, 67, 161-173.
- Hutter, K. and Koch, T., (1991). Motion of a granular avalanche in an exponentially curved chute: experiments and theoretical predictions. *Phil. Trans. R. Soc. Lond. A*, 334(1633), 93-138.
- Iverson, R.M., (2015). Scaling and design of landslide and debris-flow experiments. *Geomorphology*, 244, 9-20.
- Iverson, R.M., Logan, M., LaHusen, R.G. and Berti, M., (2010). The perfect debris flow? Aggregated results from 28 large-scale experiments. *Journal of Geophysical Research: Earth Surface*, 115(F3).
- Miura, K., Maeda, K. and Toki, S., (1997). Method of measurement for the angle of repose of sands. *Soils and Foundations*, 37(2), 89-96.
- Zhou, G.G., Ng, C.W. and Sun, Q.C., (2014). A new theoretical method for analyzing confined dry granular flows. *Landslides*, 11(3), 369-384.

No.	Referee 2's comments	Reply
1	Page 5: value of 2.0 proposed by Wendeler in 2008: PHD Thesis ETH No 17916	Reply: Thanks for your correction, we have corrected this citation error in Page 5 (Line 122-124) and Table 3.
2	Page 7: velocity of the flow only calculated by the high speed videos? Very roughly, no laser devices in front of the barrier?	Reply: The velocity of the granular flow was measured from continuous photographs taken by the side-view high-speed camera. To reduce the measuring error, the impact velocity of the granular flow is calculated from the average value of the velocities of 5 particles measured from 5 continuous photographs before the impact with the assistance of the reference lines attached to the flume. Related explanation has been added into the manuscript in Page 9 (Lines 209-213). We agree that more measuring devices will increase the accuracy of measurement.
3	Page 8: 5 m/s can be for granular flow in the correct range but I am wondering about bulk density given with 1600 kg/m ³ fitting not in the range of granular flow which normally have around 2000 kg/m ³ (page 22) and more.	Reply: We agree that the typical bulk density of granular flows is around 2000 kg/m ³ , but the testing material in our study is dry aggregate, which has a lower bulk density.
4	Page 10: Second surge not realistic for reality, because the material was already drained. How long was the time in between the two surges? In a real debris flow it happen all together very quickly, there is no time of drainage	Reply: The time interval between two tests is around 2 weeks, because we need at least 2 weeks to prepare a test. We agree that the drainage of the debris deposition should be considered in the study of multiple debris flows. In our study, the research subject is dry granular flow. Thus, drainage should not be a problem.
5	Page 12, line 279 it is Figure 12 instead of Figure 10.	Reply: Thanks for your correction, we have corrected it in the manuscript.

6	<p>Page 16: Two tests is nothing for research background and statistic interpretation. You need more tests to interpret the results correctly. Second test is not useful because front was stopped, no dynamic impact onto the barrier.</p>	<p>Reply: We agree that more tests can enhance the reliability of the quantitative conclusions drawn in this study, but it is difficult to perform more tests in a short period due to the long preparation time of a large-scale test. The granular flow in Test 2 was stopped before it can reach the flexible barrier due to the poor fluidity of dry granular flows, but it still can provide valuable data in the study of the motion and the deposition of the second surge in a multiple granular flow event.</p>
7	<p>Page 17: explain and discuss the results together with table 3 page 24. It must be more clearly explained where the results come from.</p>	<p>Reply: Thanks for the valuable comments. With the conclusions drawn from Table 3, it can be preliminarily concluded that the impact force on the flexible ring net and on the supporting structures should be estimated separately using different simple approaches. Thus, the design of a flexible barrier for debris flow mitigation can be optimized by dimensioning and designing the flexible ring net and the supporting structures individually with appropriate design loadings, which provides a safer and more economical design method.</p> <p>A specified explanation has been added into the manuscript (Lines 474 to 479).</p> <p>We have also corrected the citation error of the hydro-dynamic approach with the dynamic coefficient of 2.0 in Table 3.</p>
8	<p>Page 17: I still believe that $c=2.0$ is representing the granular impact on flexible barriers but we need more test results.</p>	<p>Reply: We agree that the hydro-dynamic approach with the dynamic coefficient of 2.0 can correctly represent the impact of a granular flow on the flexible barrier based on the comparisons in our study. More tests are under consideration to further verify the coefficients in simple approaches using different debris material such as muddy debris flows.</p>

1 **Large Scale Physical Modelling Study of a Flexible Barrier under the**
2 **Impact of Granular Flows**

3
4 by

5 **Dao-Yuan TAN**

6 Department of Civil and Environmental Engineering
7 The Hong Kong Polytechnic University, Hung Hom, Kowloon, Hong Kong, China
8 Email: t.daoyuan@connect.polyu.hk
9

10 **Jian-Hua YIN** (Chair Professor and Corresponding Author)

11 Department of Civil and Environmental Engineering
12 The Hong Kong Polytechnic University, Hung Hom, Kowloon, Hong Kong, China
13 Tel: (852) 2766-6065, Fax: (852) 2334-6389, Email: cejhyin@polyu.edu.hk
14

15 **Wei-Qiang FENG**

16 Department of Civil and Environmental Engineering,
17 The Hong Kong Polytechnic University, Hung Hom, Kowloon, Hong Kong, China
18 Email: fengweiqiang2015@gmail.com
19

20 **Jie-Qiong QIN**

21 Department of Civil and Environmental Engineering
22 The Hong Kong Polytechnic University, Hung Hom, Kowloon, Hong Kong, China
23 Email: jieqiong.qin@connect.polyu.hk
24

25 And

26 **Zhuo-Hui ZHU**

27 Department of Civil and Environmental Engineering
28 The Hong Kong Polytechnic University, Hung Hom, Kowloon, Hong Kong, China
29 Email: zhuo-hui.zhu@connect.polyu.hk
30
31

32
33
34 Manuscript submitted to *Natural Hazards and Earth System Sciences* for possible
35 publication as a Technical Paper
36
37

38 August 2018
39

40 **Abstract:**

41 Flexible barriers are being increasingly applied to mitigate the danger of debris flows.
42 However, how barriers can be better designed to withstand the impact loads of debris
43 flows is still an open question in natural hazard engineering. Here we report an
44 improved large-scale physical modelling device and the results of two consecutive
45 large-scale granular flow tests using this device to study how flexible barriers react
46 under the impact of granular flows. In the study, the impact force directly on the flexible
47 barrier and the impact force transferred to the supporting structures are measured,
48 calculated and compared. Based on the comparison, the impact loading attenuated by
49 the flexible barrier is quantified. The hydro-dynamic approaches with different
50 dynamic coefficients and the hydro-static approach are validated using the measured
51 impact forces.

52 **KEYWORDS:** Large-scale tests; granular flow; flexible barrier; impact loading

53

54 **1. Introduction**

55 Debris flows, as one of the most disastrous natural geohazards, have caused destructive
56 damage to human lives and their habitations in many countries such as USA, Japan,
57 and China (Takahashi 2014; Hungr 1995; Ishikawa *et al.* 2008; Su *et al.* 2017). In a
58 mountainous area where a large amount of loose sediment is present, multiple debris
59 flows can occur under intensive heavy rains (Xu *et al.* 2012; Yagi *et al.* 2009; Chen *et*
60 *al.* 2017). Protective systems such as concrete check dams are usually installed in areas
61 threatened by debris flows to prevent the damage (Santi *et al.* 2011). Nowadays,
62 researchers have found that flexible barriers, which were firstly used in rockfall
63 prevention, are effective to trap debris flows (Canelli *et al.* 2012; Wendeler *et al.* 2007;
64 Cui *et al.* 2015; Hu *et al.* 2006; Kwan *et al.* 2014). Compared to conventional rigid
65 concrete check dams, flexible barriers have a few obvious advantages: economical,
66 efficient in impact energy absorption, easy to be installed and adaptable to various
67 terrains (Ashwood and Hungr 2016; Wendeler and Volkwein 2015).

68

69 Physical modelling has been widely used in geotechnical engineering research because
70 of its excellent controllability in testing conditions and good reliability of testing results
71 (Paik *et al.* 2012; Wendeler *et al.* 2006; Bugnion *et al.* 2012; DeNatale *et al.* 1999).

72 Scaling is a key parameter in experiment design for studying debris flows because it
73 can affect the interaction between particles in a granular flow. In miniaturized debris
74 flows generated in small-scale tests, the effects of viscous shear resistance, friction, and
75 cohesion are over-represented, whereas the effects of excess pore-fluid pressure, which
76 are generated by debris dilation or contraction, are under-represented (Iverson 2015).

77 [With appropriate dimensional analysis, laboratory tests can be used to qualitatively](#)
78 [study behavior of the interaction between a debris flow and a flexible barrier \(Wendeler](#)

79 [and Volkwein 2015, Wendeler *et al.* 2018, Song *et al.* 2017\)](#). However, the dynamic
80 [behavior of different barrier components of a prototype flexible barrier and the stiffness](#)
81 [of the flexible ring nets applied in the field are difficult to be reliably replicated in](#)
82 [miniaturized physical models \(Wendeler *et al.* 2018\)](#). Considering the scale effects,
83 some researchers use large-scale physical models or field-scale experimental sites to
84 study debris flows (DeNatale *et al.* 1999; Wendeler 2008; Paik *et al.* 2012; Bugnion *et*
85 *al.* 2012; Iverson 2015). WSL (2010) conducted a series of full-scale tests to study the
86 interaction between multiple debris flows and a prototype flexible barrier. Large-scale
87 physical modelling tests are also selected by the authors to investigate the interaction
88 between a flexible barrier and dry granular flows.

89

90 A typical flexible barrier usually consists of two main components: a flexible ring net
91 and supporting structures (supporting posts stretching the flexible barrier, strand cables
92 and foundations supporting the posts). The impact loading from a debris flow is firstly
93 attenuated by the flexible ring net with large deformation, then transfers to the cross-
94 tension cables, which form the outline frame and stretch the ring net, and finally to the
95 posts and the supporting cables. Generally, energy dissipating elements are installed on
96 the supporting cables to reduce load peaks transferred to the foundations (Volkwein
97 2014; Wendeler *et al.* 2018). In this study, energy dissipating elements are replaced by
98 large capacity tension link transducers to accurately measure the impact loading
99 transferred to the supporting structures.

100

101 Impact loading estimation is key to the design of a flexible barrier for debris flow
102 mitigation (Volkwein *et al.* 2011). [Wendeler *et al.* \(2018\) concluded that the static](#)
103 [pressure on the flexible barrier is dominant and gradually increases with time during](#)

104 [the impact process based on the observations of field tests](#). Simple approaches are
105 commonly used by designers in impact loading estimation because they require only a
106 few parameters in the calculation. There are two widely accepted simple approaches:
107 the hydro-dynamic approach and the hydro-static approach. The hydro-dynamic
108 approach is based on momentum conservation. In this approach, the impact period is
109 taking as an ideal flow with a uniform velocity impacting the barrier and deviating
110 along the vertical direction. The impact loading is calculated from the momentum
111 change of the decelerated debris flow during the impact (Hungr *et al.* 1984; Armanini
112 1997). The hydro-static approach, on the other hand, is calculated from the earth
113 pressure of deposited debris (Rankine 1857). Both approaches adopt empirical
114 coefficients to reach a good accuracy in predicting real cases.

115

116 The estimation of impact force with the hydro-dynamic approach (Hungr *et al.* 1984)
117 is expressed as follows:

$$118 \quad F_{calculated} = \alpha \rho_{bulk} v_0^2 h w \quad (1)$$

119 where ρ_{bulk} is the bulk density of a debris flow, v_0 is the velocity of the debris flow, h is
120 the height of the debris flow, w is the width of the debris flow, which is normally
121 represented by the width of the flowing channel, and α is the dynamic coefficient.
122 Hungr *et al.* (1984) proposed a value of 1.5. Wendeler (2008) suggested a value of 0.7
123 for mud flows and 2.0 for granular flows considering the flexibility and permeability
124 of flexible barriers. Canelli et al (2012) proposed a range of values from 1.5 to 5.

125

126 The hydro-static approach (Lichtenhahn 1973; Armanini 1997) is given as follows:

$$127 \quad F_{calculated} = \kappa \rho_{bulk} g h_{deposit}^2 w \quad (2)$$

128 where κ is the static coefficient, which is suggested as 1.0 in the calculation (Kwan and

129 Cheung 2012; Wendeler *et al.* 2018). g is gravitational acceleration, and $h_{deposit}$ is the
130 deposition height of the debris flow.

131

132 Wendeler *et al.* (2018) proposed a stepwise load model to describe the impact pressures
133 on the flexible barrier during the impact process. In this model, the hydro-dynamic
134 approach with the dynamic coefficient of 0.7 for mud flows and 2.0 for granular flows
135 and the hydro-static approach with the static coefficient of 1.0 are used to calculate the
136 dynamic impact loading from the moving debris flow and the earth pressure from the
137 static debris deposition, respectively. The whole impact process was divided into three
138 impact stages: the initial impact, the filling stage and the overflow stage. In the initial
139 impact stage, there was only dynamic impact loading on the flexible barrier. In the
140 filling stage, the loading combination on the flexible barrier contained both the dynamic
141 impact loading and the static earth pressure. In the overflow stage, only the static
142 loading from the deposited debris and the overflowed debris flow exerted on the flexible
143 barrier. This method was verified by the tensile forces on the supporting cables of a
144 flexible barrier in the field tests.

145

146 However, the interaction between a flexible barrier and multiple granular flows has not
147 been fully understood. Values of the suggested coefficients used in the hydro-dynamic
148 and hydro-static approaches need to be further verified. The efficiency of loading
149 reduction by flexible barriers has not been accurately quantified. Therefore, further
150 research on the impacts of debris flows on a flexible barrier is urgently required.

151

152 This paper aims to study the motions of multiple granular flows and the performance
153 of a flexible barrier under the impact of granular flows with large-scale physical

154 modelling tests. The data from well-arranged transducers and high-speed cameras in
155 the debris flow impact tests are presented and analyzed in this paper. The motions of
156 two consecutive granular flows are described in detail. The impact forces on the flexible
157 ring net and the supporting structures of the flexible barrier are measured respectively.
158 Using the measured results, the contribution of flexibility to impact loading reduction
159 is quantified, and simple approaches with different coefficients for impact force
160 estimation are verified.

161

162 **2. Experiment setup and instrumentation**

163 *2.1 Description of the experiment apparatus*

164 A testing device is built in the Road Research Lab of the Hong Kong Polytechnic
165 University with a length of 9.5 m, a height of 8.3 m and a width of 2 m. The view of
166 the experiment setup is plotted in Fig.1. This facility can be divided into 4 main
167 components: (i) a reservoir with the capacity of 5 m³ at the top of the device, (ii) a novel
168 quick flip-up door opening system at the front vent of the reservoir, (iii) a prototype
169 flexible barrier with supporting posts and cables, and (iv) a flume linking the reservoir
170 and the flexible barrier. The prototype flexible barrier with a width of 2.48 m is made
171 up of steel rings with a diameter of 300 mm (No. ROCCO 7/3/300, Geobruigg), which
172 are commonly used in rockfall mitigation in European and Hong Kong. This ring net is
173 covered by a flexible secondary net with the mesh size of 50mm to provide a high
174 trapping rate for the granular flows. Two parallel posts that can rotate in the plane of
175 impact are installed to stretch and support the ring net, and each post is supported by
176 two inclined strand cables. The flume has a length of 7 m, an inner width of 1.5 m and
177 an inclination angle of 35 °. Side walls of the flume are made up of tempered glass to
178 provide a clear observation to the generated granular flows and their interactions with

179 the flexible barrier. Based on the parameters of the large-scale physical model built by
180 USGS (Iverson *et al.* 2010; Iverson 2015), the physical model built in the Hong Kong
181 Polytechnic University (PolyU model) can be regarded as a large-scale physical model
182 because it has similar dimensional parameters with respect to the USGS debris-flow
183 flume. Specifically, the capacity of testing material is 5 m³ in PolyU model compared
184 to 10 m³ in USGS flume, and the width of the flume is 1.5 m in PolyU model compared
185 to 2 m in USGS flume. Even though the length of the flume in PolyU model is much
186 shorter than the length of USGS flume (7 m compared to 95 m), the flume in PolyU
187 model is sufficient to generate debris flows with dynamic parameters and impact energy
188 similar to real cases. In the trial tests, the generated watery flood can reach a velocity
189 higher than 8 m/s during the flowing down.

190

191 **2.2 Instrumentation**

192 To monitor the performance of a flexible barrier under the impact of granular flows,
193 this device is instrumented with a well-arranged high-frequency measurement system.
194 Two types of transducers are installed on the flexible protection system: mini tension
195 link transducers and high capacity tension link transducers. The mini tension link
196 transducers were calibrated in the soil laboratory with a maximum loading of 20 kN.
197 The calibration is plotted in Fig.2. Those transducers are installed on the flexible ring
198 net to measure the impact force on the flexible ring net directly. Specifically, the central
199 area of the flexible ring net, which consists of 5 connected rings, is separated from the
200 main net and reconnected to the neighboring rings by 10 mini tension link transducers.
201 Fig.3 presents the measured central area and the arrangement of all the mini tension
202 link transducers on the flexible ring net. The high capacity tension link transducers with

203 a certified capacity of 50 kN are installed on the supporting cables of the posts (see
204 Fig.1 (b)). A data-logger with the capability of sampling 48 transducers at 1000 Hz
205 simultaneously is used to collect the data of all transducers. Two high-speed cameras
206 capable of capturing a resolution of 1024×768 pixels at a sampling rate of 1000 frames
207 per second are used to capture the motions of the granular flows and the deformation
208 of the flexible barrier under impact. One high-speed camera is located at the right side
209 of the barrier, and the other one is set in front of the barrier. The impact velocity of the
210 debris flow was measured from continuous photographs taken by the side-view high-
211 speed camera. To reduce the measuring error, the velocity is calculated from the
212 average velocities of 5 individual particles measured from 5 continuous photographs
213 before the impact with the assistance of the reference lines attached to the flume.

214

215 ***2.3 Experiment material and procedures***

216 The sample of material used in the tests is plotted in Fig.4, and their properties are listed
217 in Table 1. The internal friction angle of the aggregate, which is regarded having the
218 same value with the angle of repose, is measured by the pouring tests introduced by
219 Miura *et al.* (1997) and Zhou *et al.* (2014). The interface friction angle is determined
220 by the tilting plane method introduced by Hutter and Koch (1991) and Zhou *et al.*
221 (2014). Two consecutive tests, named Test 1 and Test 2 were conducted using the same
222 granular material. In test 1, the granular flow travelled via the flume and impacted an
223 empty flexible barrier. While in Test 2, the granular flow moved on the upper surface
224 of the deposition in Test 1 to simulate the second surge in multiple flows. The progress
225 of each test is described as follows. At the beginning of the test, the door was flipped
226 up in less than 0.5 s with the help of a fast door opening system to generate a uniform
227 granular flow. The datalogger started to obtain data several seconds before the

228 triggering of the granular flow to obtain initial values of all the transducers.
229 Simultaneously, the high-speed cameras started to capture the motion of the granular
230 flow and its interaction with the flexible barrier during the impact.

231

232 **3. Test results**

233 ***3.1 Motion and impact of granular flow in Test 1***

234 In test 1, the initial time of the impact has been readjusted to 0 s in all plotted data and
235 selected video frames, and the negative value of time represents the moment before the
236 interaction. By tracking the motion of the granular flow with high-speed cameras, the
237 speed of the granular flow was 5 m/s, which was relatively low compared with the
238 measured velocities from 2 m/s to 12 m/s in literatures (Arattano and Marchi 2005;
239 Prochaska *et al.* 2008; Berti *et al.* 1999). The deposition height of the granular flow and
240 the maximum horizontal deformation of the flexible barrier at different times are
241 measured from the profiles of the granular flow in photographs taken by the side-view
242 high-speed camera during the impact period (see Fig.5). It can be observed from Fig.5
243 that the front portion of the granular flow shot up, impacted the barrier directly and
244 deposited as a wedge-shaped dead zone at the bottom of the flexible barrier from 0 s to
245 1.0 s. The following granular flow climbed on the top surface of the previous stationary
246 deposition, impacted the flexible barrier, and deposited behind the barrier layer by layer.
247 After 1.0 s, the following granular front deposited behind the deposition wedge. It is
248 worth noting that the tensile force on the net keeps increasing even the deposition height
249 of the granular flow reach the maximum value. This phenomenon indicates that the
250 granular flow can continuously exert impact pressure on the flexible barrier via the
251 deposition wedge. The memasured deposition height, the maximum horizontal

252 deformation and the tensile force history of Transducer 1 change with time are plotted
253 in Fig.6. It can be seen that the deposition height of the trapped aggregate rises almost
254 linearly with time and reaches 0.55 m at the time of 1.0 s, and the horizontal
255 deformation of the barrier increases from an initial value of 0.262 m to 0.481 m at the
256 time of 1.0 s.

257

258 ***3.2 Impact loading analysis in Test 1***

259 Tensile forces recorded by the mini tension link transducers between rings are plotted
260 in Fig.7. Signals of the transducers have some noises due to the intensive impacts from
261 thousands of particles during the impact period. Thus, trend lines are added into those
262 figures to clarify the changes of tensile forces. A gradual rise of static load and two
263 dynamic impact peaks are observed in the signals of most transducers. The first impact
264 peak occurred at the beginning of the impact, and the second impact peak appeared at
265 the end of the impact. These two peaks are much smaller than the accumulated static
266 load. It is indicated that the dynamic load and the static load co-existed in the impact
267 process, and the static load was dominant. [The loading situations of the flexible barrier
268 in our study fits well with the observations of the field tests by Wendeler *et al.* \(2018\)
269 that the impact loadings on the supporting ropes increase gradually over time during
270 the impact process. Since the dynamic loading due to the oncoming debris fronts is
271 nearly constant, they concluded that the increase of the impact loading mainly attributes
272 to the incremented debris deposition.](#) Besides, transducers connected to the bottom
273 cross-tension cable (Transducer 7 and Transducer 8) show negative values, which
274 indicates that they were compressed in the impact process. Fig.8 presents typical frames
275 recorded by the side-view camera and the front-view camera combined with the signal

276 from Transducer 1. From this figure, it can be indicated that the first dynamic impact
277 peak came from the direct impact of the first debris front on the flexible barrier, and the
278 gradual increase of the static load was caused by the deposition of the aggregate. With
279 the growth of the deposition zone, the impact loading of the following granular flow
280 was finally fully resisted by the deposition cushion. Afterwards, only static earth
281 pressure of the deposition acted on the flexible barrier.

282

283 *3.3 Motion of granular flow in Test 2*

284 The second granular flow was triggered after Test 1 to simulate the second flow in a
285 multiple debris flow event. In Test 2, the granular flow travelled on the top surface of
286 the deposition in Test 1 and came to rest without reaching the net. The motion of the
287 granular flow in Test 2 is plotted in Fig.9. In that figure, the initiated time of the granular
288 flow is readjusted to 0 s. It can be found that the granular flow had a thick front when
289 it was firstly triggered, then the thickness kept decreasing during movement. Based on
290 the recording of the side-view camera, the side-view of depositions in the two tests and
291 the velocity change of the granular flow with the flowing distance in Test 2 are plotted
292 in Fig.10. The thickness and velocity of the front reduced dramatically with the increase
293 of the moving distance and finally stopped at 0.7 m before the flexible barrier.
294 Correspondingly, no impact force and deformation increment of the flexible barrier
295 were recorded by the transducers and the high-speed cameras. The reason for the flow
296 stopping before the flexible barrier is the large basal friction of the rough interface
297 between the moving granular flow and the deposition and the low fluidity of the dry
298 granular flow. The multi-flow tests show that the impact from the latter arrived debris

299 flows can be attenuated or eliminated by the resistance from the deposition of the
300 previous debris flow in a multiple debris flow event.

301

302 **4. Data analysis**

303 *4.1 Direct measurement of the impact force on the flexible barrier*

304 As mentioned above, the central area is separated from the main ring net and
305 reconnected to neighboring net rings by mini tension link transducers. Two assumptions
306 are made to simplify the measurement of the impact loading on a flexible ring net. The
307 deformation of the ring net is assumed similar to a membrane, and the deformation in
308 the measured area is assumed cone symmetric. Based on the assumptions, the loading
309 situation in the cross-section of the measured area which contains Transducer i and
310 Transducer $i+1$ is analyzed and shown in Fig.11. Thus, the impact force on the cross-
311 section can be calculated with the following equation:

$$312 \quad F_{impact,i,i+1} = F_{tensile,i} \cdot \cos \frac{\theta}{2} + F_{tensile,i+1} \cdot \cos \frac{\theta}{2} \quad (3)$$

313 where $F_{tensile,i}$ and $F_{tensile,i+1}$ are the maximum tensile forces on Transducer i and
314 Transducer $i+1$ installed in the measured area, θ is the included angle between the
315 opposite transducers, $F_{impact,i,i+1}$ is the calculated impact force on this cross-section.
316 Since the deformation in the measured area is assumed cone symmetric, θ is a constant
317 in all cross-sections formed by two opposite transducers. Thus, for the measured area
318 with n transducers, the maximum impact force, $F_{measured}$, can be calculated with the
319 following equation:

$$320 \quad F_{measured} = \cos \frac{\theta}{2} \cdot \sum_{i=1}^{i=n} F_{tensile,i} \quad (4)$$

321 In our study, the maximum tensile forces on all transducers are measured and plotted
 322 in Fig.12, and θ can be measured from the photograph taken at the moment of the largest
 323 deformation as shown in Fig.13.

324

325 The impact pressure from the granular flow is assumed to be uniformly distributed in
 326 the cross-section area of the flume width multiplied by the height of the debris
 327 deposition, which covers the measured central area. [The uniformly distributed impact
 328 loading on the flexible ring net has been proved by back-calculation using the tensile
 329 forces and deformations of the horizontal supporting cables of the flexible barrier in
 330 field tests \(Wendeler *et al.* 2018\).](#) Combined with Eq. 4, the following equation is given
 331 to calculate the distributed impact loading on a flexible ring net:

$$332 \quad F_{impact} = F_{measured} \cdot \frac{A_{impact}}{A_{measured}} = \cos \frac{\theta}{2} \cdot \sum_{i=1}^{i=n} F_{tensile,i} \cdot \frac{A_{impact}}{A_{measured}} \quad (5)$$

333 where A_{impact} and $A_{measured}$ represent the actual impact cross-section area and the
 334 measured central area in the test as shown in Fig.12. All the parameters and calculated
 335 results are listed in Table 2.

336

337 **4.2 Calculation of Loading Reduction Rate (LRR)**

338 The flexible ring net is supported by two posts that can rotate in the plane of the flow
 339 direction, and each post is supported by two inclined steel strand cables. Therefore, the
 340 impact force transferred from the flexible barrier to the supporting posts can be
 341 calculated from the tensile forces carried by the supporting cables in the direction of
 342 impact. Based on the symmetrical arrangement of the cables and the posts with respect
 343 to the flexible barrier, as plotted in Fig.14 (a), the loading situations of the posts and
 344 the supporting cables located on both sides of the flexible barrier are also symmetrical

345 when they are under a uniform impact pressure. Thus, the left post and its supporting
346 cables: Cable A Left and Cable B Left are selected as the analysis objects. The force
347 analysis of the supporting cables is divided into two steps:

348 Firstly, forces on Cable A Left and Cable B Left are decomposed into components in
349 the rotation plane of the post based on the top-view sketch (see Fig.14(a)):

350
$$F_{AL,H} = F_{AL} \cdot \cos \alpha \quad (6)$$

351
$$F_{BL,H} = F_{BL} \cdot \cos \beta \quad (7)$$

352 where F_{AL} and F_{BL} are the measured maximum tensile forces on Cable A Left and Cable
353 B Left during the impact, $F_{AL,H}$ and $F_{BL,H}$ are the components of F_{AL} and F_{BL}
354 decomposed in the rotation plane of the left post, and α , β are the included angles
355 between Cable A, Cable B and the rotation plane of the post.

356

357 Secondly, based on the calculated $F_{AL,H}$ and $F_{BL,H}$, components of the tensile forces on
358 Cable A Left and Cable B Left in the direction of impact can be calculated based on the
359 left-side-view sketch (see Fig.14 (b)):

360
$$F_{AL,impact} = F_{AL,H} \cdot \cos \gamma \quad (8)$$

361
$$F_{BL,impact} = F_{BL,H} \cdot \cos \delta \quad (9)$$

362 where $F_{AL,impact}$ and $F_{BL,impact}$ are the components of tensile forces on Cable A Left and
363 Cable B Left in the direction of impact, and γ , δ are the included angles between Cable
364 A, Cable B and the direction of impact.

365

366 It is defined that the direction of the supporting force, which is opposite to the direction
 367 of the impact force, is the positive direction. Thus, the components of the tensile forces
 368 on the left cables in the direction of impact (F_L) can be calculated by substituting Eqs.
 369 (6) and (7) into Eqs. (8) and (9):

$$370 \quad \begin{aligned} F_L &= F_{BL,impact} - F_{AL,impact} = F_{BL,H} \cdot \cos \delta - F_{AL,H} \cdot \cos \gamma \\ &= F_{BL} \cdot \cos \delta \cdot \cos \beta - F_{AL} \cdot \cos \gamma \cdot \cos \alpha \end{aligned} \quad (10)$$

371 Finally, based on the conservation of angular momentum and the symmetrical
 372 arrangement of the cables and the posts with respect to the flexible barrier, the
 373 equivalent impact force can be calculated from the tensile forces on the supporting
 374 cables with the following equation:

$$375 \quad F_{Cables, equivalent} = \frac{l_{post}}{l_{impact}} [(F_{BL} + F_{BR}) \cdot \cos \delta \cdot \cos \beta - (F_{AL} + F_{AR}) \cdot \cos \gamma \cdot \cos \alpha] \quad (11)$$

376 where $F_{Cables, equivalent}$ is the equivalent impact force calculated from the tensile forces on
 377 the supporting cables, l_{post} is the distance between the rotation fulcrum of the post and
 378 the connecting point of the cables, l_{impact} is the distance between the rotation fulcrum of
 379 the post and the equivalent impact height of the granular flow. F_{AL} , F_{AR} , F_{BL} , and F_{BR}
 380 are the measured maximum tensile forces on the supporting cables. Their values are
 381 presented in Fig.13. All parameters, as well as the calculated results, are listed in Table
 382 2.

383

384 It is found that flexibility of flexible barriers makes an obvious contribution to the
 385 reduction of the impact loading from a debris flow (Volkwein 2014; Song *et al.* 2017).
 386 Since almost all the debris material was trapped in this study, the load reduction mainly
 387 attributes to the large deformation of the flexible ring net during the impact. To quantify

388 the contribution of flexibility to impact loading reduction, the Loading Reduction Rate
389 (LRR) of the flexible barrier is defined as:

$$390 \quad LRR = \frac{F_{impact} - F_{Cables, equivalent}}{F_{impact}} \cdot 100\% \quad (12)$$

391 LRR in the granular flow tests is calculated and presented in Table 2. It is found that
392 around 28 % of the impact loading from the dry granular flow in Test 1 was attenuated
393 by the flexible barrier.

394

395 ***4.3 Comparison of simple approaches with measured impact forces***

396 Two widely accepted simple approaches for impact force estimation: hydro-dynamic
397 approach and hydro-static approach (Kwan and Cheung 2012; Volkwein 2014; Song *et*
398 *al.* 2017; Ashwood and Hungr 2016; Wendeler 2008; Wendeler *et al.* 2018) are
399 compared in this section to validate their applications in the design of flexible barriers.
400 To quantify the accuracies of the simple approaches, Relative Error (RE) is usually
401 defined as:

$$402 \quad RE = \left| \frac{F_{calculated} - F_{measured}}{F_{measured}} \right| \times 100\% \quad (13)$$

403 where $F_{calculated}$ represent the calculated impact force of the simple approach, which is
404 obtained by integrating the parameters listed in Table 1 and Table 2 into the hydro-
405 dynamic and hydro-static approaches listed in Table 3. [In the table, two dynamic](#)
406 [coefficients suggested by Wendeler \(2008\): 0.7 for mud flow and 2.0 for granular flow](#)
407 [and a static coefficient of 1.0 are utilized.](#) $F_{measured}$ is the measured impact force on
408 different components of the flexible barrier.

409 The calculated results are validated using the measured impact forces on the flexible
410 ring net and on the supporting structures. The validation results are quantified with the

411 value of Relative Error. The results of the calculation and the validation are listed in
412 Table 3. Compared with the measured impact force on the flexible ring net directly, the
413 hydro-dynamic approach with the dynamic coefficient of 2.0 has the best performance
414 in estimating the impact force on the flexible ring net with a small deviation of 5.8 %,
415 which verifies the dynamic coefficient suggested by Wendeler (2008) for granular
416 flows. The reduced dynamic coefficient of 0.7 for debris flows with lower densities
417 (lower than 1900 kg/m³), on the other hand, obviously under-estimated the loading on
418 the flexible ring net by 50%. The reduction of the dynamic coefficient takes account of
419 the dewatering and penetration of small particles during the impact based on lab tests
420 and field observations (Wendeler 2008; Wendeler and Volkwein 2015; Wendeler *et al.*
421 2018). Therefore, the under-estimation of the impact loading could attribute to the all
422 trapped granular material by the secondary mesh net in our dry granular flow impact
423 tests based on the observations of the impact process with the high-speed cameras.
424 While the hydro-static approach with the static coefficient of 1.0 fits quite well with the
425 measured impact force on the supporting structures. This is reasonable since part of the
426 dynamic impact from the granular flow can be attenuated by the flexible ring net, and
427 the static loading can be fully transferred to the supporting structures. This phenomenon
428 is also proved by the gradually increased tensile forces on Cable B Left and Cable B
429 Right shown in Fig.13 (b). Thus, in the design of a flexible barrier for debris flow
430 mitigation, the hydro-dynamic approach and the hydro-static approach can be used in
431 the design and the selection of the flexible ring net and the supporting structures,
432 respectively. Even the dynamic coefficients and the static coefficient are verified by the
433 data of large-scale tests in this study, more tests are required to further verify and select
434 suitable coefficients before they can be used in the design.

435

436 **5. Conclusions**

437 In this paper, an improved large-scale physical modelling facility for debris flow
438 research and a well-arranged high-frequency measurement system are introduced.
439 Using this device, two tests were performed to study the behavior of a flexible barrier
440 subjected to the impacts of granular flows. From the experimental data and their
441 analysis, key findings and conclusions are summarized and presented as below:

442 (a) In Test 1, the front of the granular flow impacted the flexible ring net directly,
443 deposited behind the barrier layer by layer, and formed a deposition wedge in the
444 first second. After 1.0 s, the following granular flow deposited behind the
445 deposition wedge.

446 (b) The static loading and the dynamic loading co-existed in the impact process, and
447 the static loading was dominant. The static loading attributed to the gradual
448 deposition of aggregate, and the dynamic loading was caused by the impact of the
449 debris front. The latter arrived granular front applied impact loading on the flexible
450 barrier via the deposition wedge. With the deposition of aggregate, the stationary
451 debris formed a cushion behind the barrier and attenuated all the impact loading
452 from the following granular front.

453 (c) In Test 2, the second granular flow in a multiple flow event was performed. The
454 velocity and the flow depth of the granular flow decreased during movement, and
455 the front stopped before it can reach the flexible barrier due to the large basal
456 friction between the moving granular flow and the granular deposition and the poor
457 fluidity of the dry granular flow.

458 (d) The impact loading on a flexible ring net was directly measured from the tensile
459 forces on the central area of the flexible ring net. In Test 1, the measured maximum

460 impact force on the flexible ring net was 10.96 kN.

461 (e) The contribution of flexibility to impact loading reduction is quantified by
462 introducing the Loading Reduction Rate (LRR). By calculating the impact loading
463 transferred to the supporting structures, it can be concluded that almost 28 % of the
464 impact loading from the granular flow was attenuated by the flexible ring net.

465 (f) From the comparisons of the hydro-dynamic approach and the hydro-static
466 approach with the measured impact forces on different components, it is found that
467 the hydro-dynamic approach with the dynamic coefficient of 2.0 fits well with the
468 measured impact force on the flexible ring net, and the hydro-static approach with
469 the static coefficient of 1.0 has a good performance in estimating the impact force
470 on the supporting structures.

471

472 The motion characteristics of the multiple granular flows indicate that the motion and
473 the impact of the following debris flow can be resisted or eliminated by the deposition
474 of previous debris flow. By applying the LRR and suitable impact loading estimation
475 approaches, the impact force on the flexible ring net and on the supporting structures
476 can be estimated separately by using appropriate simple approaches. Thus, the design
477 of a flexible barrier for debris flow mitigation can be optimized by dimensioning and
478 designing different components with different designed loadings, which provides a
479 safer and more economical design method. In the future, the tests of rapid debris flows
480 will be conducted to investigate the behavior of debris flows and examine the
481 performance of a flexible barrier under the impact of rapid debris flows.

482

483 **Acknowledgement**

484 The authors acknowledge the financial support from Research Institute for Sustainable
485 Urban Development of The Hong Kong Polytechnic University (PolyU). The work in
486 this paper is also supported by a National State Key Project “973” grant (Grant No.:
487 2014CB047000) (sub-project No. 2014CB047001) from Ministry of Science and
488 Technology of the People’s Republic of China, a CRF project (Grant No.:
489 PolyU12/CRF/13E) from Research Grants Council (RGC) of Hong Kong Special
490 Administrative Region Government of China. The financial supports from PolyU
491 grants (1-ZVCR, 1-ZVEH, 4-BCAU, 4-BCAW, 4-BCB1, 5-ZDAF) are acknowledged.
492 This paper is also supported by Research Centre for Urban Hazards Mitigation of
493 Faculty of Construction and Environment of PolyU.

494

495 **References**

- 496 Arattano, M., and Marchi, L.: Measurements of debris flow velocity through cross-
497 correlation of instrumentation data. *Natural Hazards and Earth System Science*,
498 5(1), 137-142, 2005.
- 499 Armanini, A., and Michiue, M.: *Recent developments on debris flows* (Vol. 64).
500 Springer, 1997.
- 501 Ashwood, W., and Hungr, O. Estimating total resisting force in flexible barrier
502 impacted by a granular avalanche using physical and numerical modeling.
503 *Canadian Geotechnical Journal*, 53(10), 1700-1717, 2016.
- 504 Berti, M., Genevois, R., Simoni, A. and Tecca, P.R. Field observations of a debris flow
505 event in the Dolomites. *Geomorphology*, 29(3-4), 265-274, 1999.
- 506 Bugnion, L., McArdell, B. W., Bartelt, P., and Wendeler, C. Measurements of hillslope
507 debris flow impact pressure on obstacles. *Landslides*, 9(2), 179-187, 2012.

508 Canelli, L., Ferrero, A. M., Migliazza, M., and Segalini, A. Debris flow risk mitigation
509 by the means of rigid and flexible barriers-experimental tests and impact analysis.
510 *Natural Hazards and Earth System Sciences*, 12(5), 1693, 2012.

511 Chen, H.X., Zhang, L.M., Gao, L., Yuan, Q., Lu, T., Xiang, B. and Zhuang, W.L.
512 Simulation of interactions among multiple debris flows. *Landslides*, 14(2), 595-
513 615, 2017.

514 Cui, P., Zeng, C. and Lei, Y. Experimental analysis on the impact force of viscous
515 debris flow. *Earth Surface Processes and Landforms*, 40(12), 1644-1655, 2015.

516 DeNatale, J. S., Iverson, R. M., Major, J. J., LaHusen, R. G., Fiegel, G. L., and Duffy,
517 J. D. Experimental testing of flexible barriers for containment of debris flows. US
518 Department of the Interior, US Geological Survey, 1999.

519 Hungr, O. A model for the runout analysis of rapid flow slides, debris flows, and
520 avalanches. *Canadian Geotechnical Journal*, 32(4), 610-623, 1995.

521 Hungr, O., Morgan, G.C., and Kellerhals, R. Quantitative Analysis of Debris Torrent
522 Hazards for Design of Remedial Measures. *Canadian Geotechnical Journal* 21(4):
523 663–77, 1984.

524 Hutter, K. and Koch, T. Motion of a granular avalanche in an exponentially curved
525 chute: experiments and theoretical predictions. *Phil. Trans. R. Soc. Lond. A*,
526 334(1633), 93-138, 1991.

527 Ishikawa, N., Inoue, R., Hayashi, K., Hasegawa, Y., and Mizuyama, T. Experimental
528 approach on measurement of impulsive fluid force using debris flow model. *na*,
529 2008.

530 Iverson, R.M., Logan, M., LaHusen, R.G. and Berti, M. The perfect debris flow?
531 Aggregated results from 28 large-scale experiments. *Journal of Geophysical*
532 *Research: Earth Surface*, 115(F3), 2010.

533 Iverson, R.M. Scaling and design of landslide and debris-flow experiments.
534 *Geomorphology*, 244, 9-20, 2015.

535 Kwan J.S.H. and Cheung R.W.M. Suggestions on design approaches for flexible
536 debris-resisting barriers. Discussion Note No. DN 1/2012, Geotechnical
537 Engineering Office, Hong Kong, 90, 2012.

538 Kwan, J.S.H., Chan, S.L., Cheuk, J.C.Y. and Koo, R.C.H. A case study on an open
539 hillside landslide impacting on a flexible rockfall barrier at Jordan Valley, Hong
540 Kong. *Landslides*, 11(6), 1037-1050, 2014.

541 Lichtenhahn, C. Die Berechnung von Sperren in Beton und Eisenbeton [Die design of
542 barriers made of concrete and reinforced concrete]. Kolloquium über
543 Wildbachsperren. Mitteilungen der Forstlichen Bundesanstalt Wien. Heft, 102, 91-
544 127. (in German), 1973.

545 Miura, K., Maeda, K. and Toki, S. Method of measurement for the angle of repose of
546 sands. *Soils and Foundations*, 37(2), 89-96, 1997.

547 Paik, J., Son, S., Kim, T., and Kim, S. A real-scale field experiment of debris flow for
548 investigating its deposition and entrainment. In AGU Fall Meeting Abstracts, 2012.

549 Prochaska, A.B., Santi, P.M., Higgins, J.D. and Cannon, S.H. A study of methods to
550 estimate debris flow velocity. *Landslides*, 5(4), 431-444, 2008.

551 Rankine, W. On the stability of loose earth. *Philosophical Transactions of the Royal*
552 *Society of London*, Vol. 147, 9-27, 1857.

553 Santi, P. M., Hewitt, K., VanDine, D. F., and Cruz, E. B. Debris-flow impact,
554 vulnerability, and response. *Natural hazards*, 56(1), 371-402, 2011.

555 Song, D., Choi, C. E., Ng, C. W. W., and Zhou, G. G. D. Geophysical flows impacting
556 a flexible barrier: effects of solid-fluid interaction. *Landslides*, 1-12, 2017.

557 Su, L.J., Xu, X.Q., Geng, X.Y. and Liang, S.Q. An integrated geophysical approach for
558 investigating hydro-geological characteristics of a debris landslide in the
559 Wenchuan earthquake area. *Engineering Geology*, 219, 52-63, 2017.

560 Takahashi, T. Debris flow: mechanics, prediction and countermeasures. CRC press,
561 2014.

562 Volkwein, A. Flexible debris flow barriers. Design and application. WSL Berichte.
563 Issue 18, 29, 2014.

564 Volkwein, A., Wendeler, C., and Guasti, G. Design of flexible debris flow barriers. In
565 5th International Conference debris-flow hazard mitigation. Mechanics, prediction
566 and assessment. Padua, Italy 1093-1100, 2011.

567 Wendeler, C. S. I. Murgangrückhalt in Wildbächen. Grundlagen zu Planung und
568 Berechnung von flexiblen Barrieren. ETH, 2008.

569 Wendeler, C., and Volkwein, A. Laboratory tests for the optimization of mesh size for
570 flexible debris-flow barriers. *Natural Hazards and Earth System Sciences*, 15(12),
571 2015.

572 Wendeler, C., McArdell, B. W., Rickenmann, D., Volkwein, A., Roth, A., and Denk,
573 M. Field testing and numerical modeling of flexible debris flow barriers. In
574 Proceedings of international conference on physical modelling in geotechnics,
575 Hong Kong, 2006.

576 [Wendeler, C., Volkwein, A., McArdell, B.W. and Bartelt, P. Load model for designing](#)
577 [flexible steel barriers for debris flow mitigation. *Canadian Geotechnical Journal*,](#)
578 [\(ja\), 2018.](#)

579 Wendeler, C., Volkwein, A., Roth, A., Denk, M., and Wartmann, S. Field
580 measurements and numerical modelling of flexible debris flow barriers. *Debris-*
581 *Flow Hazards Mitig. Mech. Predict. Assess.* Millpress, Rotterdam, 681-687, 2007.

582 WSL. Report on testing SL-100 a protection system against shallow landslides, 2010.

583 Xu, Q., Zhang, S., Li, W.L. and Van Asch, T.W. The 13 August 2010 catastrophic
584 debris flows after the 2008 Wenchuan earthquake, China. *Natural Hazards and*
585 *Earth System Sciences*, 12, 201-216, 2012.

586 Yagi, H., Sato, G., Higaki, D., Yamamoto, M., and Yamasaki, T. Distribution and
587 characteristics of landslides induced by the Iwate–Miyagi Nairiku earthquake in
588 2008 in Tohoku District, Northeast Japan. *Landslides* 6(4):335–344, 2009.

589 Zhou, G.G., Ng, C.W., and Sun, Q.C. A new theoretical method for analyzing confined
590 dry granular flows. *Landslides*, 11(3), 369-384, 2014.

591

Tables

Table 1. Main properties of aggregate used in the test

Main properties	Values
<i>The total volume of aggregate in Test 1 and Test 2 (m³)</i>	4
<i>Particle diameters (mm)</i>	15 ~ 30
<i>Internal friction angle (°)</i>	36
<i>Interface friction angle (°) (between aggregate and painted steel plate)</i>	28
<i>Bulk density (kg/m³)</i>	1600

Table 2. Values of measured parameters and calculated results in Test 1

Parameters and results	Values
<i>Moving speed (m/s)</i>	5
<i>Included angle θ ($^{\circ}$)</i>	130
<i>A_{measured} (m²)</i>	0.644
<i>A_{impact} (m²)</i>	1.44
$\sum_{i=1}^{i=n} F_{tensile,i}$ (kN)	11.59
<i>F_{measured} (kN)</i>	4.9
<i>l_{impact} (m)</i>	0.242
<i>l_{post} (m)</i>	2.7
<i>h_{debirs} (m)</i>	0.086
<i>h_{deposit} (m)</i>	0.58
α ($^{\circ}$)	62
β ($^{\circ}$)	24
γ ($^{\circ}$)	76
δ ($^{\circ}$)	60
<i>F_{AL} (kN)</i>	0.062
<i>F_{AR} (kN)</i>	0.062
<i>F_{BL} (kN)</i>	0.79
<i>F_{BR} (kN)</i>	0.79
<i>F_{Cables, equivalent} (kN)</i>	7.89
<i>F_{impact} (kN)</i>	10.96
<i>Loading Reduction Rate (LRR) (%)</i>	28.01

Table 3. Comparisons of the calculated impact forces using simple approaches with the measured impact forces on different components of a flexible barrier in Test 1

Simple approaches for impact force estimation	Calculated impact force (kN)	RE with impact force on the flexible net (%)	RE with impact force on the supporting structures (%)
		$F_{impact}=10.96$ kN	$F_{Cables, equivalent} =7.89$ kN
$F_{calculated} = \alpha \rho_{bulk} v_0^2 h w$ <i>(hydro-dynamic approach with $\alpha=0.7$)</i> <i>(for muddy debris flows with lower densities)</i> <i>(Wendeler 2008)</i>	3.61	67.1	54.3
$F_{calculated} = \alpha \rho_{bulk} v_0^2 h w$ <i>(hydro-dynamic approach with $\alpha=2$)</i> <i>(for granular flows)</i> <i>(Wendeler 2008)</i>	10.32	5.8	30
$F_{calculated} = \kappa \rho_{bulk} g h_{deposit}^2 w$ <i>(hydro-static approach with $\kappa=1$)</i> <i>(Kwan and Cheung 2012)</i>	7.92	27.7	0.38

Figure lists

Figure 1. (a) side view of a large-scale physical model design (unit in mm) and (b) photograph of the physical modelling facility constructed at a site in Hong Kong

Figure 2. Calibration of a tension link transducer

Figure 3. (a) schematic diagram of a flexible barrier and (b) front view of the flexible barrier with numbered tension link transducers between rings and the measured area in the physical model (unit in m)

Figure 4. Aggregate samples in the granular flow impact tests (unit in mm)

Figure 5. Side profiles of deposited aggregate at different times in Test 1

Figure 6. Relation between the deposition height of the granular flow, horizontal deformation of the flexible barrier and tensile force of Transducer 1 *v.s.* time in Test 1

Figure 7. Recorded forces *v.s.* time by the mini tension link transducers between rings in Test 1

Figure 8. Interpretation of the typical video frames in Test 1 recorded by (a) the side-view camera and (b) the front-view camera with the data of tensile force from Transducer 1

Figure 9. Motion of the granular flow in Test 2

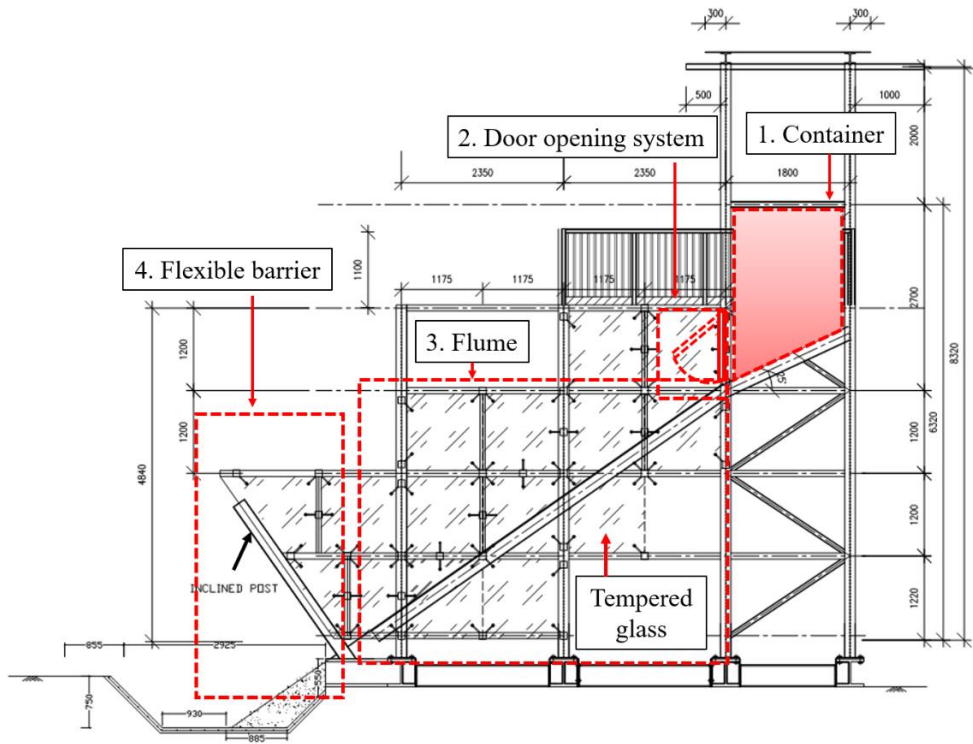
Figure 10. Side profile of the depositions in Test 1 and Test 2 and the velocity change of the granular flow in Test 2 with the moving distance

Figure 11. (a) sketch of the flexible barrier under the impact of a granular flow and (b) the simplified force analysis of the measured area in the cross-section of Transducer i and Transducer $i+1$

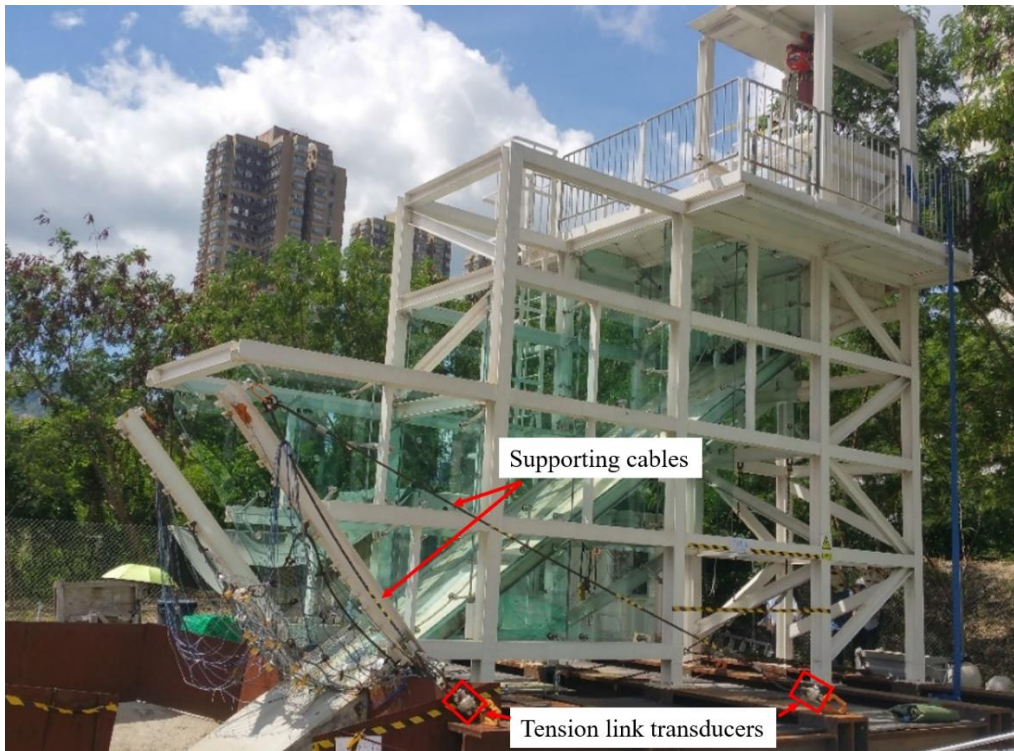
Figure 12. Sketch of the impact and measured area in Test 1 and the maximum tensile forces measured from 10 mini tension link transducers under the impact of the granular flow (unit in m)

Figure 13. (a) photograph at the instant of the largest deformation with measured parameters and (b) recorded forces and time by the tension link transducers on the supporting cables in Test 1

Figure 14. (a) top-view and (b) left-side-view of sketches with the force analysis of the posts and cables



(a)



(b)

Figure 1. (a) side view of a large-scale physical model design (unit in mm) and (b) photograph of the physical modelling facility constructed at a site in Hong Kong

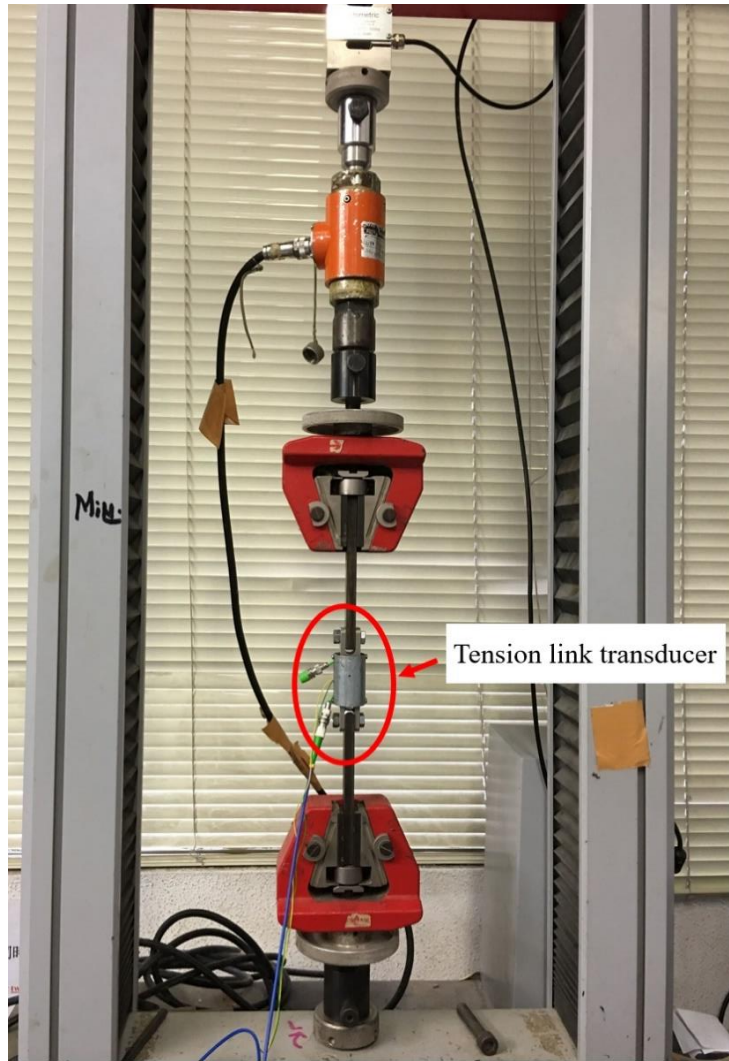
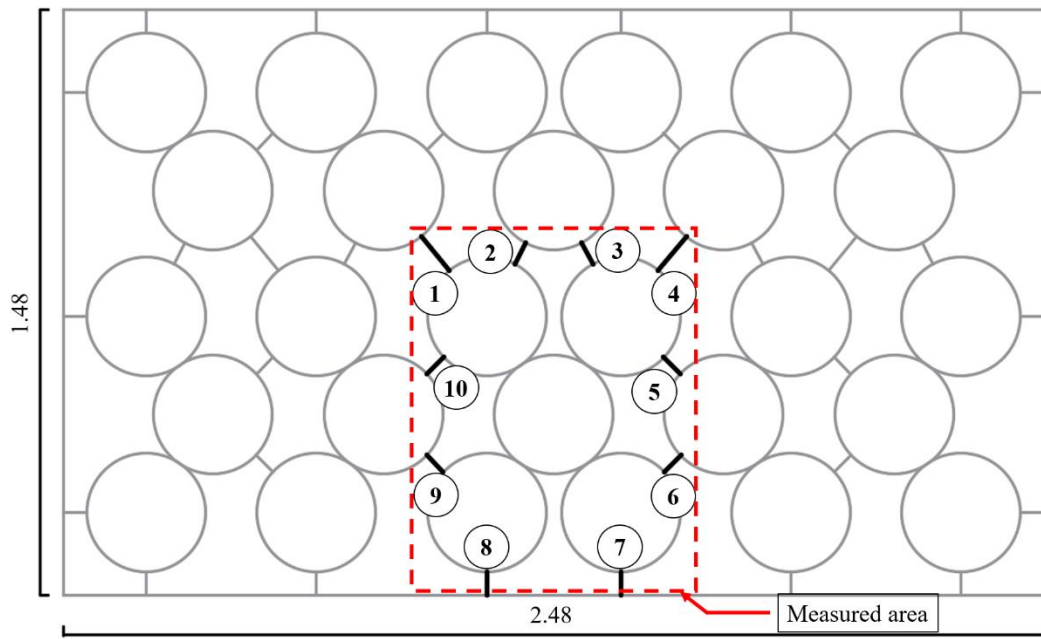
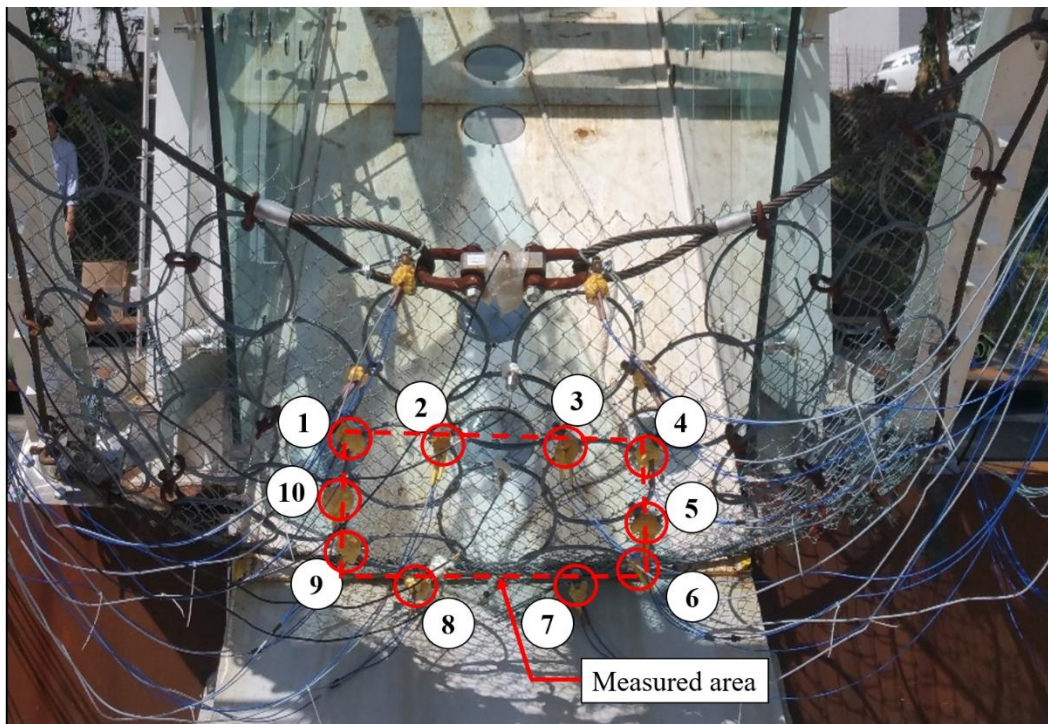


Figure 2. Calibration of a tension link transducer



(a)



(b)

Figure 3. (a) schematic diagram of a flexible barrier and (b) front view of the flexible barrier with numbered tension link transducers between rings and the measured area in the physical model (unit in m)



Figure 4. Aggregate samples in the granular flow impact tests (unit in mm)

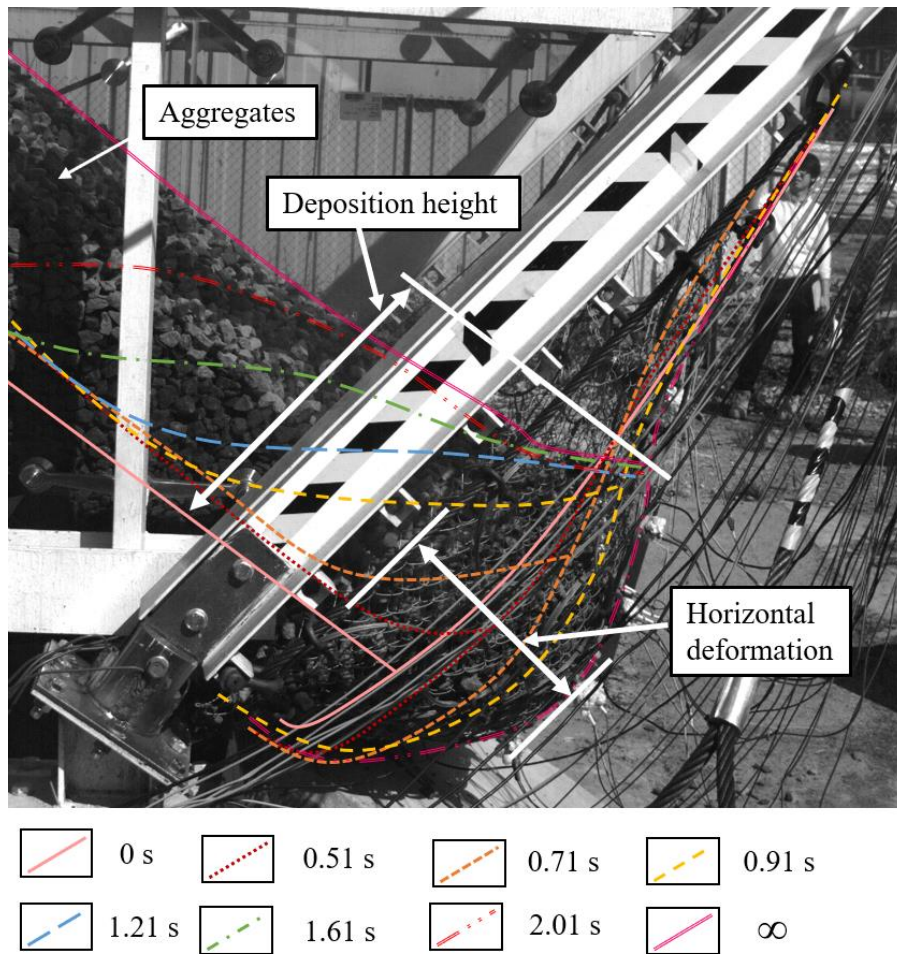


Figure 5. Side profiles of deposited aggregate at different times in Test 1

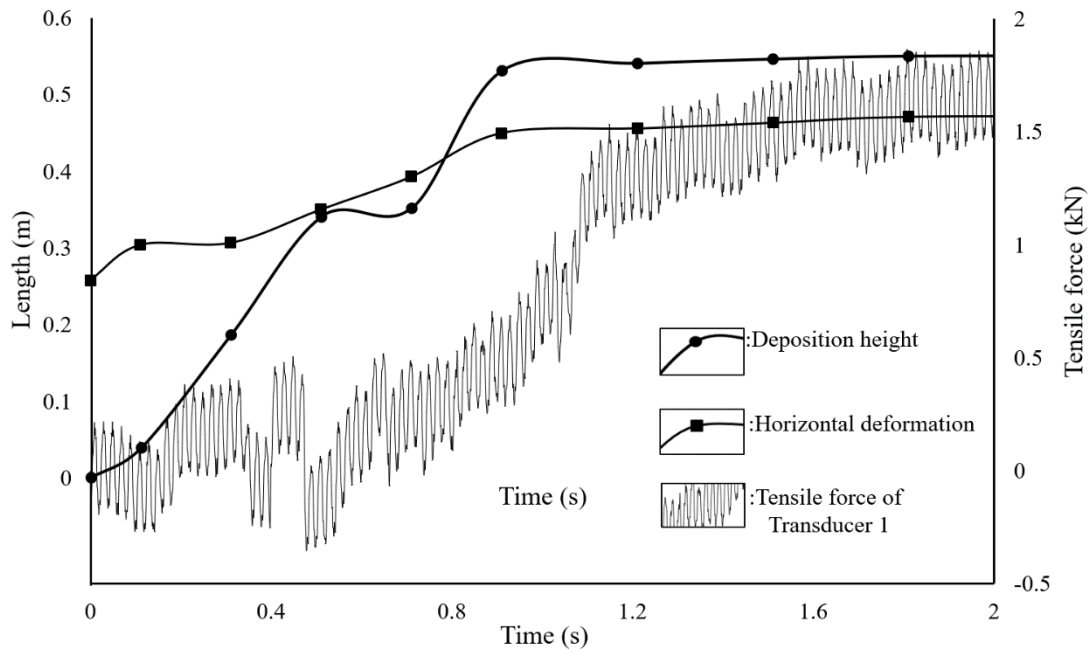


Figure 6. Relation between the deposition height of the granular flow, horizontal deformation of the flexible barrier and tensile force of Transducer 1 v.s. time in Test 1

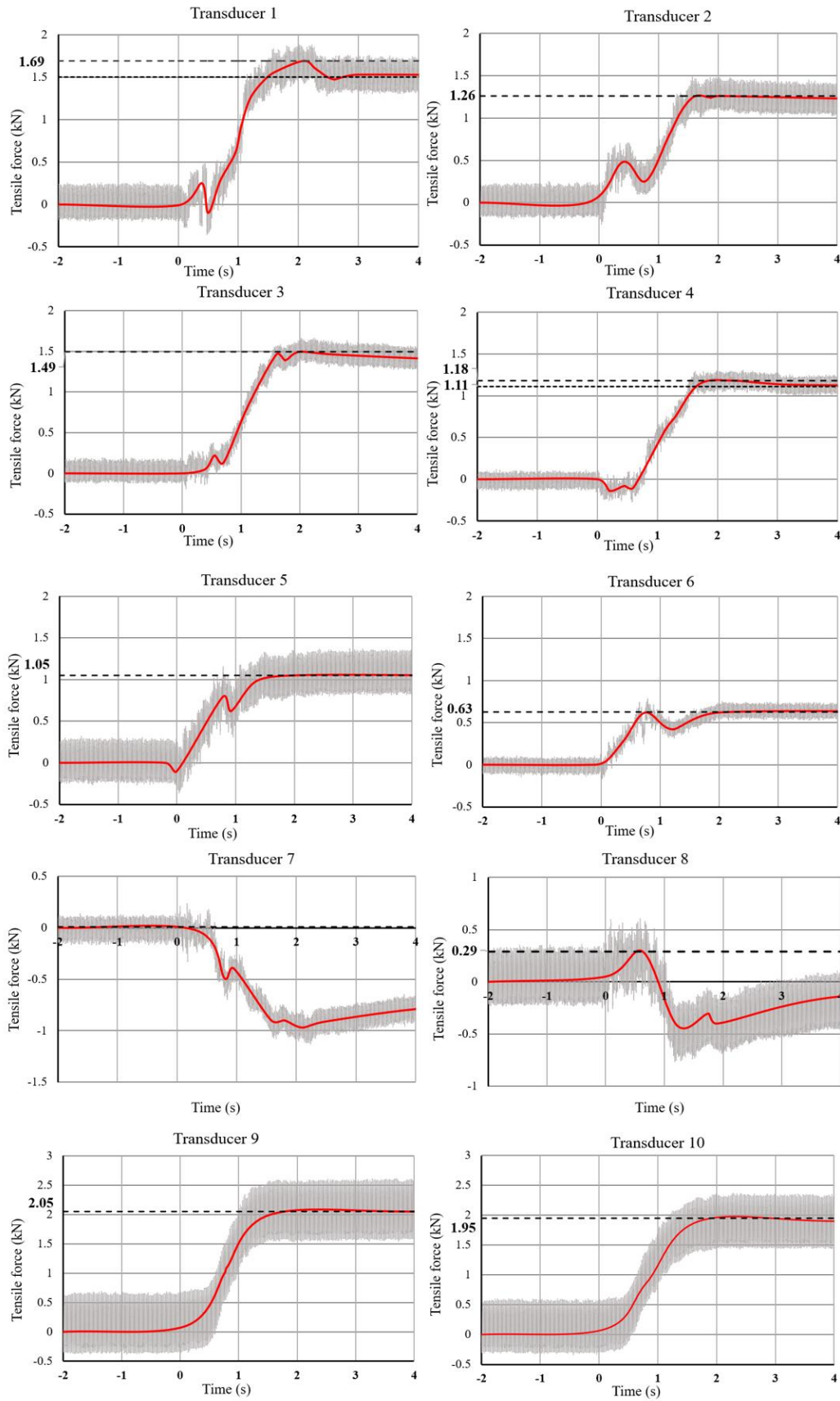
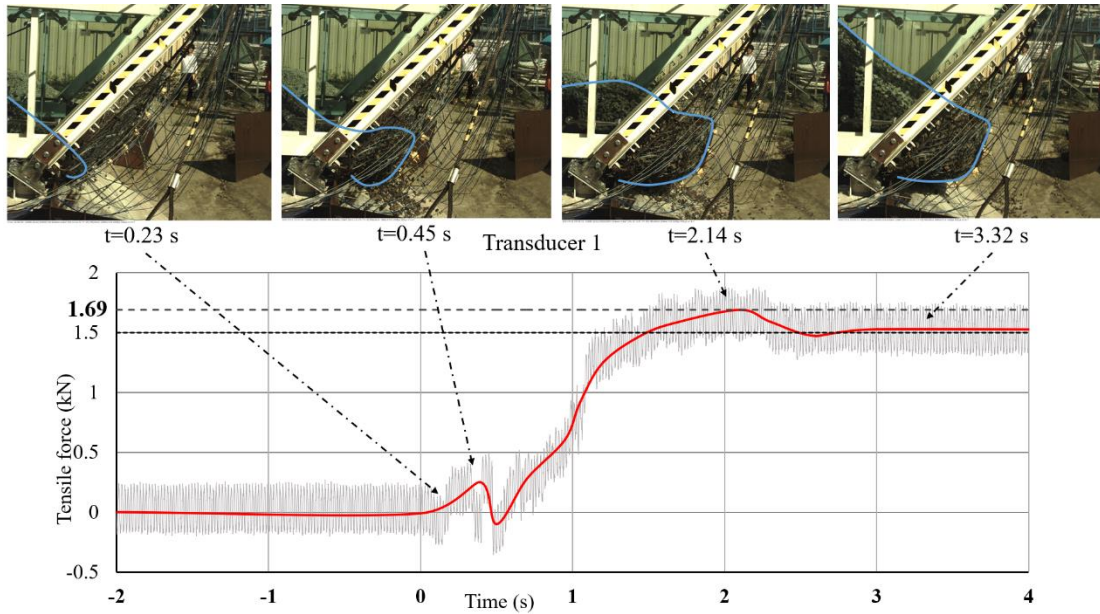
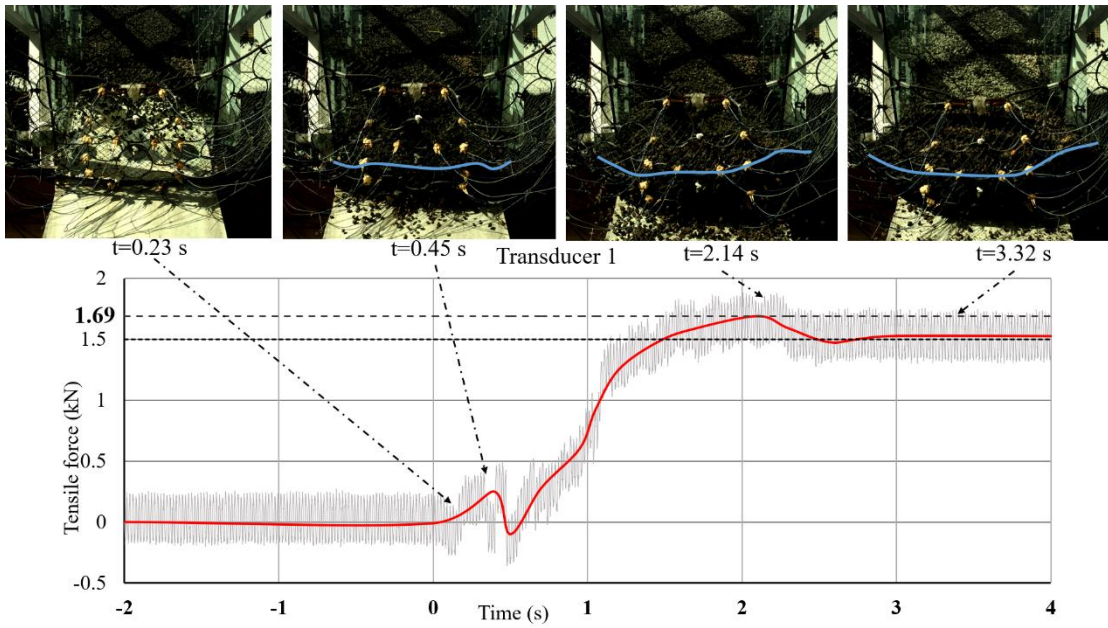


Figure 7. Recorded forces *v.s.* time by the mini tension link transducers between rings in Test 1



(a)



(b)

Figure 8. Interpretation of the typical video frames in Test 1 recorded by (a) the side-view camera and (b) the front-view camera with the data of tensile force from Transducer 1

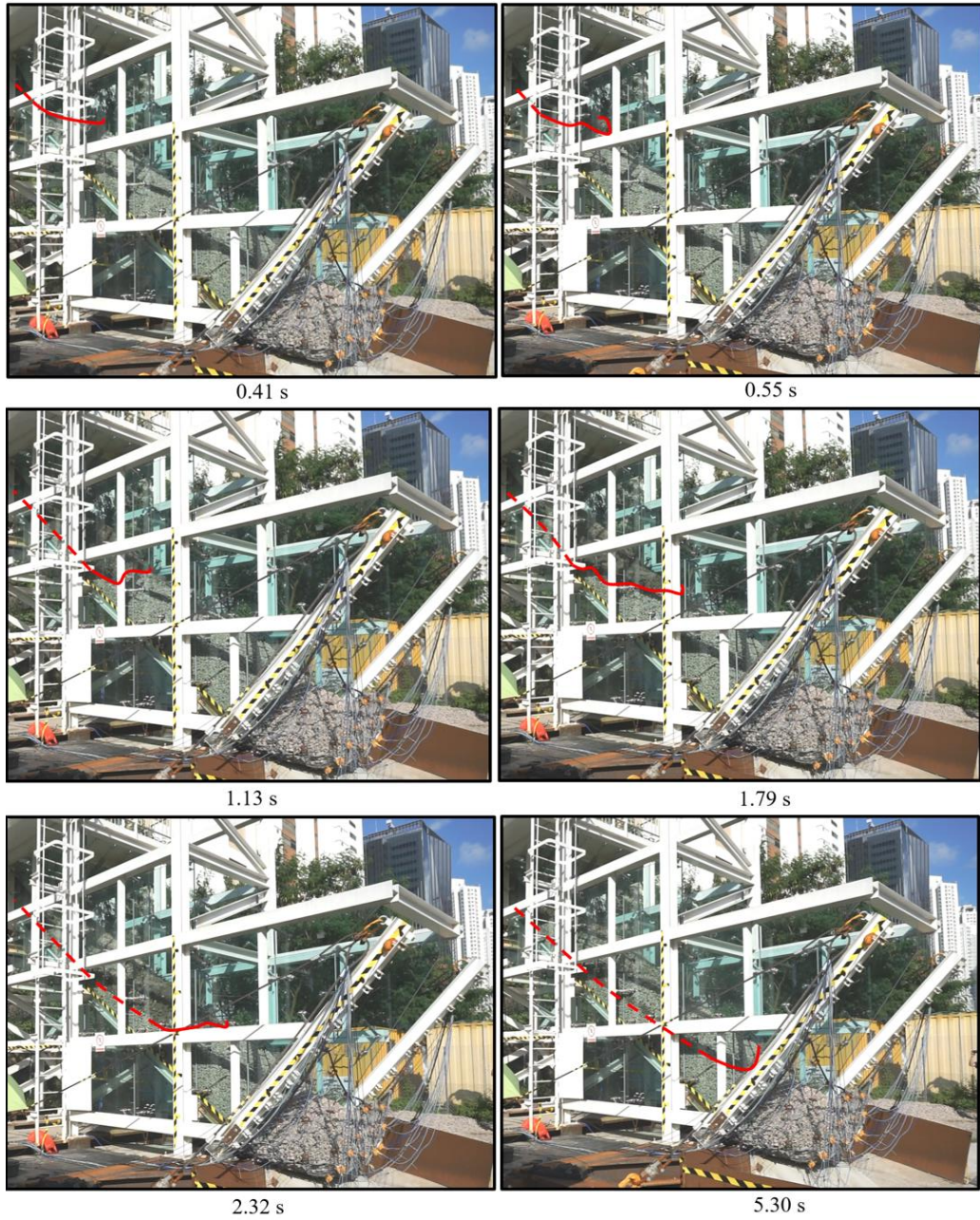


Figure 9. Motion of the granular flow in Test 2

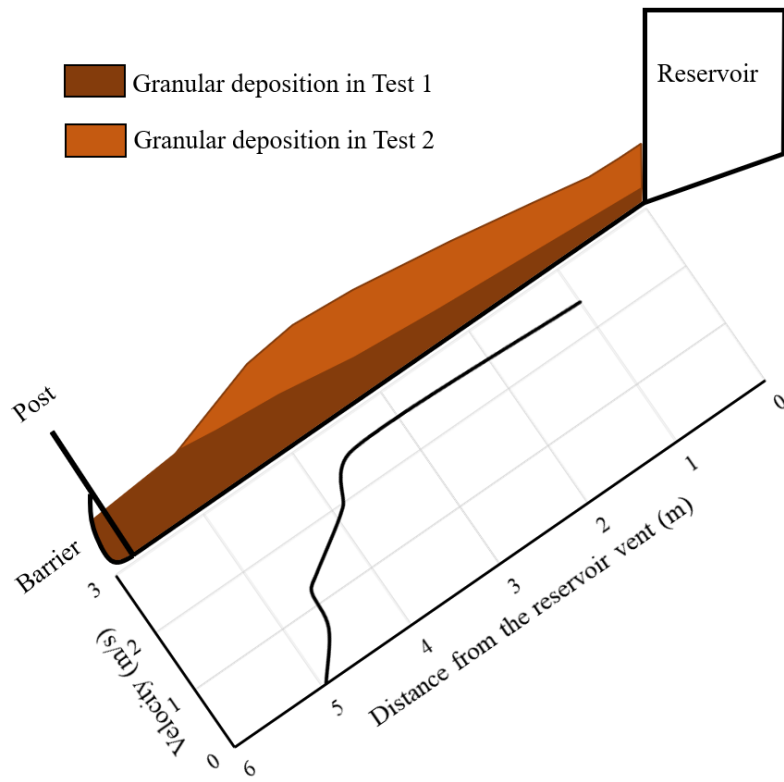


Figure 10. Side profile of the depositions in Test 1 and Test 2 and the velocity change of the granular flow in Test 2 with the moving distance

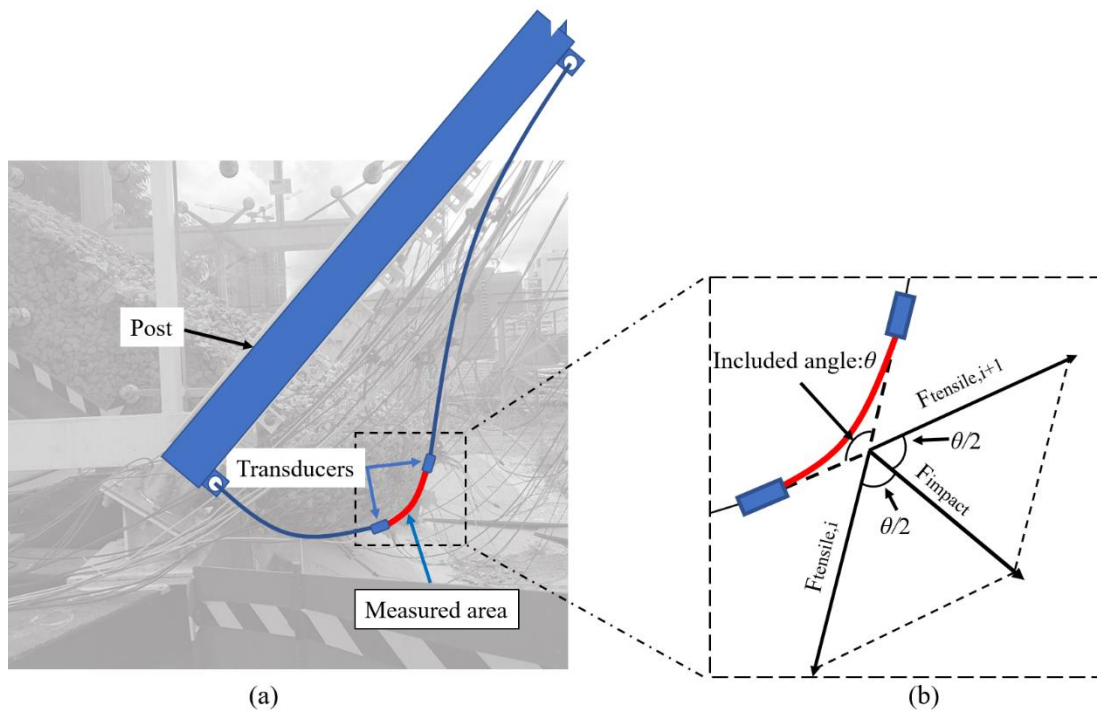


Figure 11. (a) sketch of the flexible barrier under the impact of a granular flow and (b) the simplified force analysis of the measured area in the cross-section of Transducer i and Transducer $i+1$

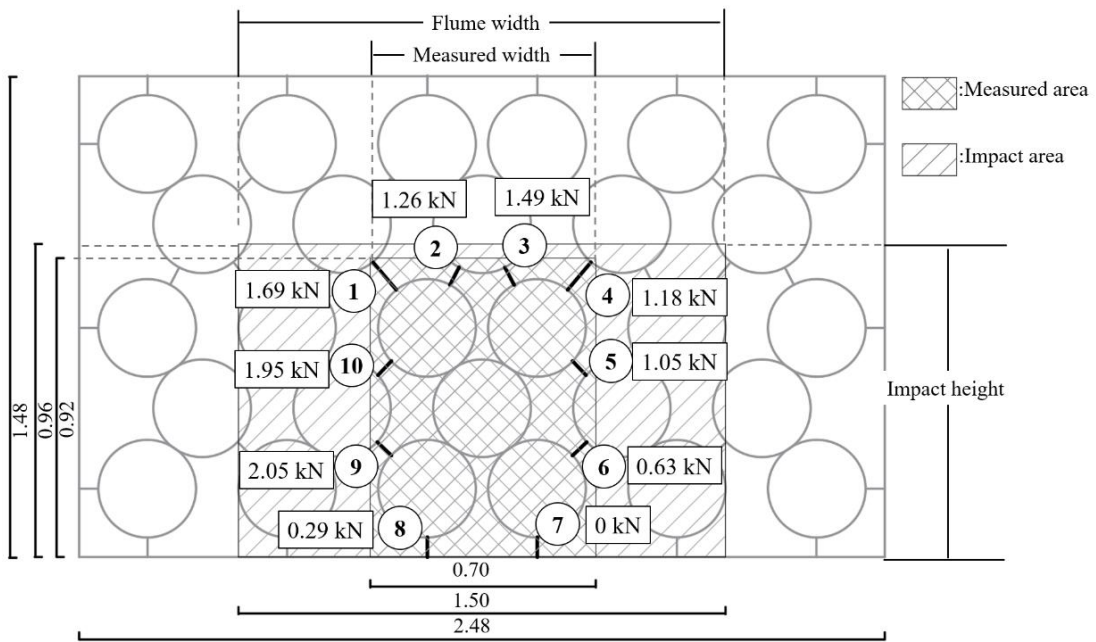
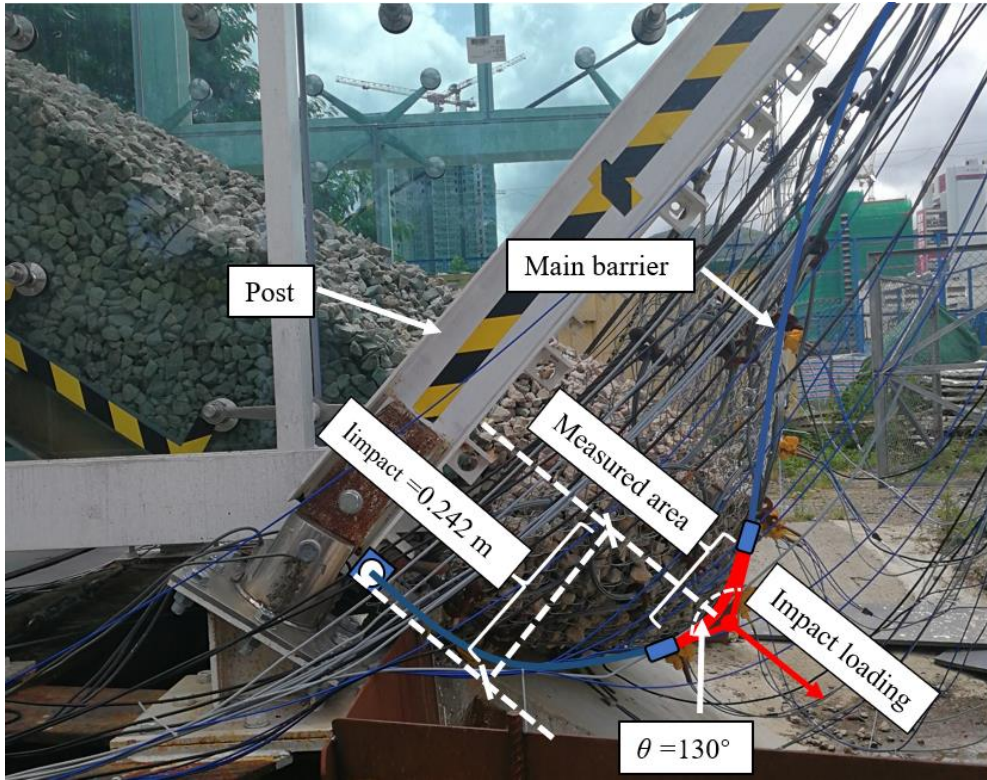
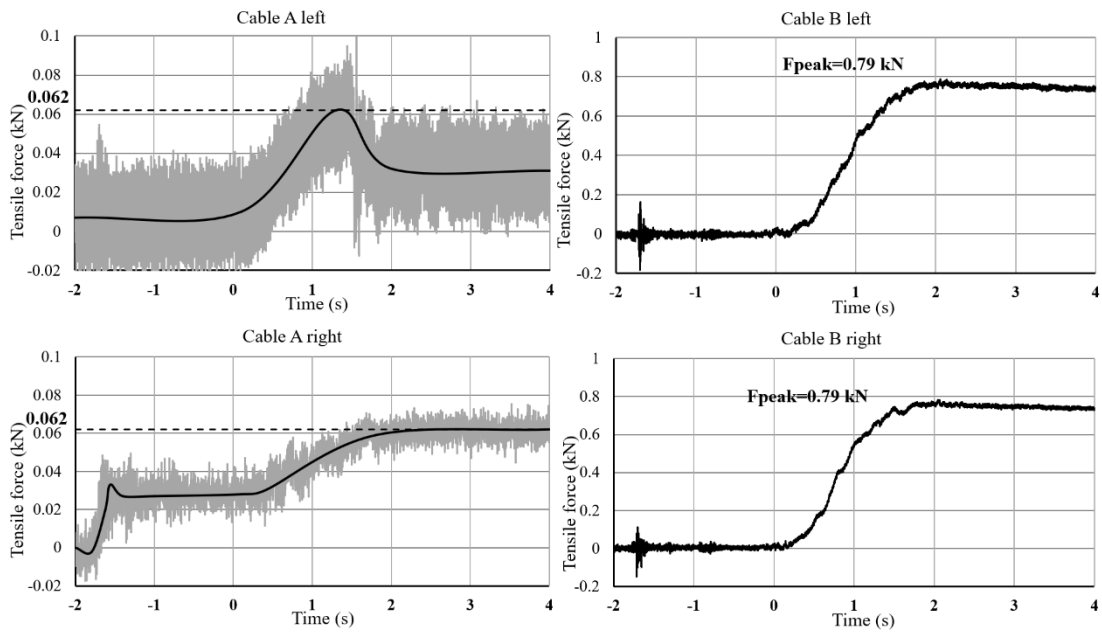


Figure 12. Sketch of the impact and measured area in Test 1 and the maximum tensile forces measured from 10 mini tension link transducers under the impact of the granular flow (unit in m)

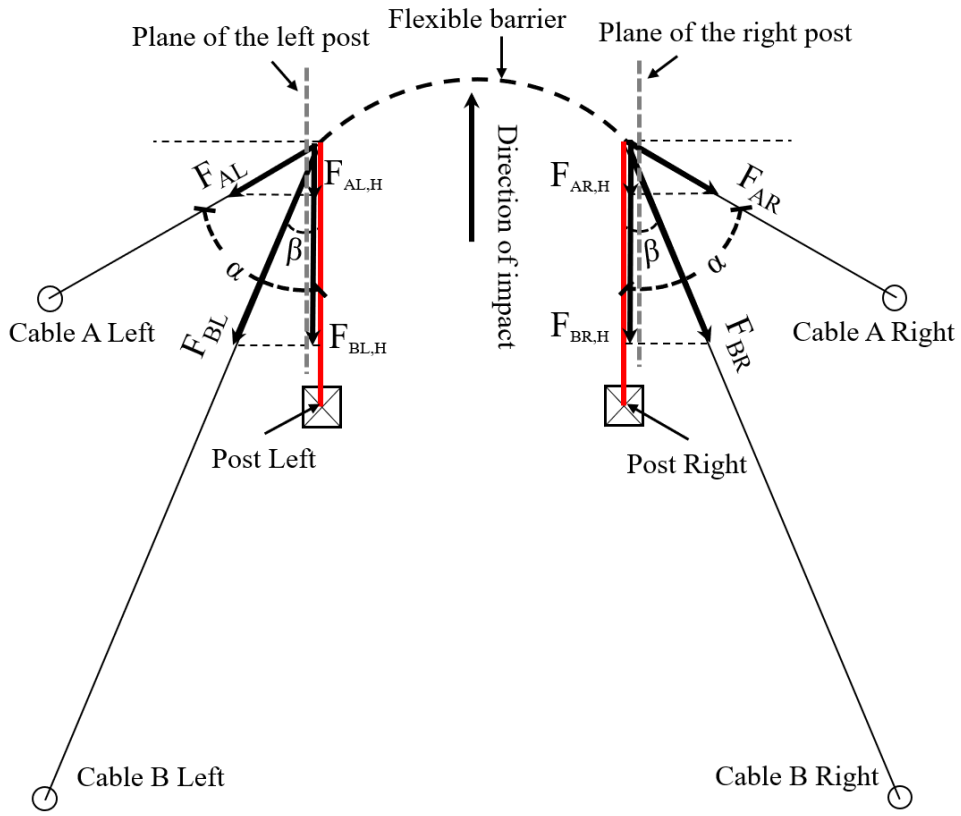


(a)

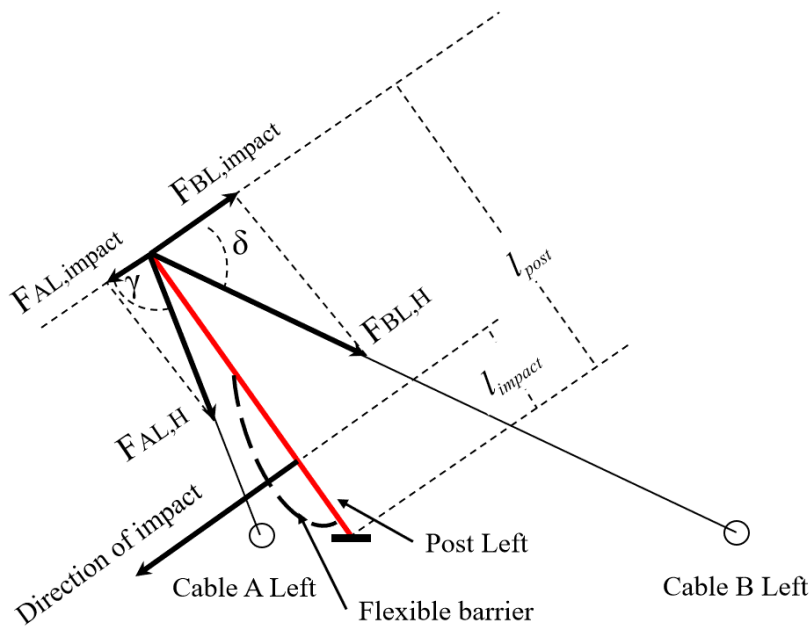


(b)

Figure 13. (a) photograph at the instant of the largest deformation with measured parameters and (b) recorded forces and time by the tension link transducers on the supporting cables in Test 1



(a)



(b)

Figure 14. (a) top-view and (b) left-side-view of sketches with the force analysis of the posts and cables